© 2018. Published by The Company of Biologists Ltd | Journal of Cell Science (2018) 131, jcs216317. doi:10.1242/jcs.216317

RESEARCH ARTICLE

Cell injury triggers actin polymerization to initiate epithelial restitution

Eitaro Aihara[1,*], Neisha M. Medina-Candelaria[1], Hikaru Hanyu[1], Andrea L. Matthis[1], Kristen A. Engevik[1], Christine B. Gurniak[2], Walter Witke[2], Jerrold R. Turner[3], Tongli Zhang[1] and Marshall H. Montrose[1,*]

ABSTRACT

The role of the actin cytoskeleton in the sequence of physiological epithelial repair in the intact epithelium has yet to be elucidated. Here, we explore the role of actin in gastric repair *in vivo* and *in vitro* gastric organoids (gastroids). In response to two-photon-induced cellular damage of either an *in vivo* gastric or *in vitro* gastroid epithelium, actin redistribution specifically occurred in the lateral membranes of cells neighboring the damaged cell. This was followed by their migration inward to close the gap at the basal pole of the dead cell, in parallel with exfoliation of the dead cell into the lumen. The repair and focal increase of actin was significantly blocked by treatment with EDTA or the inhibition of actin polymerization. Treatment with inhibitors of myosin light chain kinase, myosin II, trefoil factor 2 signaling or phospholipase C slowed both the initial actin redistribution and the repair. While Rac1 inhibition facilitated repair, inhibition of RhoA/Rho-associated protein kinase inhibited it. Inhibitors of focal adhesion kinase and Cdc42 had negligible effects. Hence, initial actin polymerization occurs in the lateral membrane, and is primarily important to initiate dead cell exfoliation and cell migration to close the gap.

KEY WORDS: Actin, Epithelial cell, Repair, Cell migration, Gastric organoid

INTRODUCTION

The actin cytoskeleton plays an important role in maintaining cellular integrity as well as coordinating cellular motility. Particularly, actin is known to drive cell protrusions that lead to cell migration, implicating a role for actin dynamics in the repair of damage to an epithelium. In fact, several previous results have demonstrated that F-actin increases at the leading edge in several epithelial wound models (Bement et al., 1993; Kuipers et al., 2014; Osada et al., 1999; Russo et al., 2005; Tamada et al., 2007).

The physiological significance of the actin dynamics in wound repair is to lead cell migration by providing the force (Levayer and Lecuit, 2012; Stricker et al., 2010), in collaboration with myosin II (i.e. the actomyosin ring) (Bement et al., 1993; Kuipers et al., 2014; Tamada et al., 2007), to push damaged cells from the cell layer and enable the neighboring cells to cover the denuded area of damage. This actomyosin contractility is regulated by phosphorylated myosin light chain (MLC, also known as MYL), which is activated by MLC kinase (MLCK) (Russo et al., 2005). Upstream in this signaling cascade, the Rho/Rho-associated protein kinases (ROCK1 and ROCK2, hereafter denoted ROCK) regulate MLC phosphorylation. It has been suggested that ROCK acts as a trigger of actomyosin ring assembly (Hall, 1998; Russo et al., 2005). In contrast, during cell migration, cell protrusions, including lamellipodia or filopodia, are formed as a result of the rearrangement of actin filaments induced by activation of Rac1 or Cdc42, respectively, (Hall, 1998). Thus, signaling via Rho family proteins impacts on actin dynamics, implicating their central role in the repair of damage. Furthermore, focal adhesion kinase (FAK, also known as PTK2) impacts on cell migration by controlling focal contacts with cell–cell and cell–extracellular matrix, as well as affecting Rho family activities (Mitra et al., 2005).

Many migration assays have been performed in monolayers using several cell lines. Induction of small wounds, by means of two-photon laser, UV light or manual scraping, leads relatively quickly to recruitment of F-actin and myosin, as well as actomyosin contraction, resulting in purse-string wound closure (Bement et al., 1993; Russo et al., 2005; Tamada et al., 2007). In the established Madin–Darby canine kidney (MDCK) cell line, focal wound healing has been shown to be a two-stage process of cell death followed by migrating cells causing extrusion of the dead cell (Kuipers et al., 2014). However, less is known about how such results relate to outcomes *in vivo*, from primary epithelial cultures, or from gastrointestinal cell types. In gastrointestinal systems, gastric epithelial wound repair has been studied in cultured primary rabbit gastric epithelium, where macroscopic wound closure was evaluated in response to a physically 'scratched' area within the culture dish. Such wound closure takes place over 24–48 h, utilizing a mixture of cell migration and cell proliferation (Ranta-Knuuttila et al., 2002; Watanabe et al., 1994a). These classic scratch wound assays lack the ability to show interaction between dead cells and their intact neighboring cells. In these *x-y* monolayer culture settings, wound closure is observed from the top of the cells, making it difficult to assess the ongoing repair processes that restore normal epithelial morphology after epithelial continuity is restored and to differentiate the localized area where actin assembly occurs along the apical to basal axis of the cells.

In vivo, it is believed that, in response to epithelial injury of a small region or programmed cell death, neighboring cells migrate to close the gap, concurrent with the exfoliation of the dead cell into lumen (Aihara and Montrose, 2014; Marchiando et al., 2011). This sequence is a natural physiological process for repair of small wounds that is dependent on cell migration, but not proliferation, and is frequently observed in the gastrointestinal epithelium (Aihara and Montrose, 2014; Marchiando et al., 2011). Actin also plays important roles in the healing of big injuries, such as gastric ulcer; in fact, that the inhibition of actin polymerization delays epithelial

[1]Department of Pharmacology and Systems Physiology, University of Cincinnati, Cincinnati, OH 45267, USA. [2]Institute of Genetics, University of Bonn, Bonn, Germany. [3]Departments of Pathology and Medicine, Brigham and Women's Hospital and Harvard Medical School, Boston, MA 02115, USA.

*Authors for correspondence (aiharaeo@uc.edu; mhm@uc.edu)

E.A., 0000-0003-1160-4929; N.M.M.-C, 0000-0002-7059-1905; M.H.M., 0000-0002-1847-0276

Received 31 January 2018; Accepted 21 July 2018

Journal of Cell Science (2018) 131, jcs216317. doi:10.1242/jcs.216317

healing *in vivo* (Banan et al., 1996). This importance of actin cytoskeleton dynamics in the gastric epithelial healing has previously been inferred from wound repair experiments *in vitro* using a rat gastric epithelial cell line (RGM1) and primary rabbit gastric epithelial cells (Nguyen et al., 2007; Osada et al., 1999; Paehler Vor der Nolte et al., 2017; Pai et al., 2001; Watanabe et al., 1994a). However, the molecular mechanisms of actin dynamics underlying the repair of damage are largely unknown in gastric epithelial cells.

Recently three-dimensional (3D) primary epithelial cell cultures, known as organoids, have been established and widely used (Bartfeld and Clevers, 2017; Sato et al., 2009). Gastric organoids (gastroids) physiologically mimic *in vivo* gastric epithelium (Schumacher et al., 2015a,b; Stange et al., 2013); therefore, we considered that gastroids could be useful for cell migration assays, replicating *in vivo* gastric epithelial cells. We previously showed that gastroids are useful as a restitution model that could replicate physiological responses (Schumacher et al., 2015a). In the present study, we investigate the actin cytoskeleton dynamics in normal epithelium of *in vivo* gastric tissue and *in vitro* gastroids following two-photon-induced damage.

RESULTS

We utilized mice expressing the human GFP–actin (HuGE) transgene, solely using heterozygotes that express the GFP–actin fusion protein as only 1–3% of the total cellular actin (Gurniak and Witke, 2007). By using intravital confocal imaging of the gastric surface *in vivo* in anesthetized mice, we observed GFP–actin homogeneously expressed in the surface epithelium and most abundantly near the plasma membrane (Fig. S1A). In gastric organoids (gastroids) created from the gastric corpus tissue of HuGE mice, GFP–actin is also uniformly expressed in the gastroid epithelium and in the same juxta-membrane locations as seen in native tissue (Fig. S1B).

Phalloidin staining confirmed that the localization of total actin was indistinguishable between gastroids created from GFP–actin-negative or -positive mice (Fig. S1C). The tight junction protein ZO-1 (also known as TJP1) is expressed in the apical junction. F-actin staining was most abundant at the apical and lateral membranes, and we observed the actin scaffold network at the apical membrane where the ZO-1 is in the same plane (Fig. S1C, asterisk, also shown in *x-z* images shown at bottom of panel). These results suggest that HuGE mice are a valid model to monitor actin distribution, and that gastroids faithfully reflect the actin distribution of native tissue.

Ca^{2+}-dependent actin dynamics during *in vivo* gastric repair

As previously described (Aihara et al., 2014; Starodub et al., 2008; Xue et al., 2010), high-intensity 730 nm two-photon photodamage (PD) was used to induce damage of three to five cells at the gastric surface epithelium *in vivo*. Tracking damage size in the HuGE mice, identified by reflectance and lack of NAD(P)H, showed gastric epithelial damage was repaired within ∼15 min (Fig. 1A,B). The GFP–actin intensity measured in the viable epithelial cells adjacent to the damaged area (Fig. 1A,B) revealed a transient decrease in response to damage, followed by a more sustained increase, especially within the leading edge of migrating cells. In contrast, GFP–actin intensity did not change in the cells >100 µm away from the damaged site (Fig. 1B), suggesting that actin specifically assembles ithe leading edge of migrating cells. Consistent with previous findings (Aihara et al., 2013), repair of damage was significantly inhibited by chelation of Ca^{2+} (addition of 10 mM HEDTA to luminal perfusate; Fig. 1C,D). Additionally, HEDTA blocked the increase of GFP–actin, suggesting that extracellular Ca^{2+} plays an important role in regulation of actin dynamics (Fig. 1E,F).

Actin dynamics and actin source during gastric epithelial repair *in vitro*

In the *in vivo* animal restitution model, subcellular actin dynamics could not be tracked at the single-cell level due to tissue motion and epithelial orientation, and it was impossible to find the damaged area in fixed tissue after experiments. Therefore, we applied two-photon damage to gastroids, a 3D primary culture of the gastric epithelium.

In response to two-photon-induced damage of the perinuclear region of a single cell in HuGE gastroids, GFP–actin intensity increased within ∼1 min in the lateral membrane next to the damaged area, and subsequently tracked the cellular contraction or migration inward to close the gap at the basal pole of the dead cell (Fig. 2A–C; Movie 1). This led to exfoliation of the dead cell into the gastroid lumen (Fig. 2A). The actin dynamics are a local response, as GFP intensity did not change in cells that were >20 µm from the damage site cells during repair (Fig. 2C). Similar to what was seen in native tissue, the closure of the damaged area was completed within ∼15 min (Fig. 2C). We also observed spontaneous natural cell shedding in the gastroids. During this event, GFP intensity increased, followed by cell exfoliation (Fig. S1D), replicating the repair process induced by photodamage. Evidence shows that the single-cell gastroid photodamage model matches important features of native tissue and normal cell replacement processes.

We performed multiple damage inductions to ask whether the increased actin originates solely from the damaged cell, and whether the pool of actin impacts the capacity for repair. In one protocol, after a first cycle of damage and repair, a second damage was imposed on the opposite side of a migrating cell that had already mounted an increase in actin. After this second damage, the increase of GFP–actin was delayed in the lateral membrane area adjacent to the new damage (Fig. S2A,B; Movie 2) and the repair of damage was significantly slower (Fig. S2C,D). In a second protocol, the middle cell had two neighboring cells that were damaged simultaneously. In this model, increases in GFP–actin in the both sides of the lateral membrane of the middle intact cell were diminished and repair was delayed (Fig. S3). These results suggest that actin availability within the restituting cell is a source of increased actin that can limit repair.

A mathematical model of actin-mediated gastric epithelial repair

We constructed a mathematical model in order to have a framework to understand the linkages within the complex temporal orchestration of actin recruitment, dead cell extrusion and damage area closure (Fig. 2D). In the model, a damage signal initiates recruitment of available actin into a branching network. This process is assumed to be fast and not to involve the synthesis of new proteins. The temporal simulations of the constructed model have recaptured the temporal order of the observed events (Fig. S4). The damaged area significantly decreases before the dead cell moves away (Fig. 2E). This implies a temporal coordination between damaged area closure and dead cell extrusion. During migrating cell protrusion, the actin network generates physical force, which in turn leads to the acceleration of the extrusion of the dead cell during the early stage. Subsequently, the cell deaccelerates due to the resistance force it experiences after the dead cell is far from the actin network

Journal of Cell Science (2018) 131, jcs216317. doi:10.1242/jcs.216317

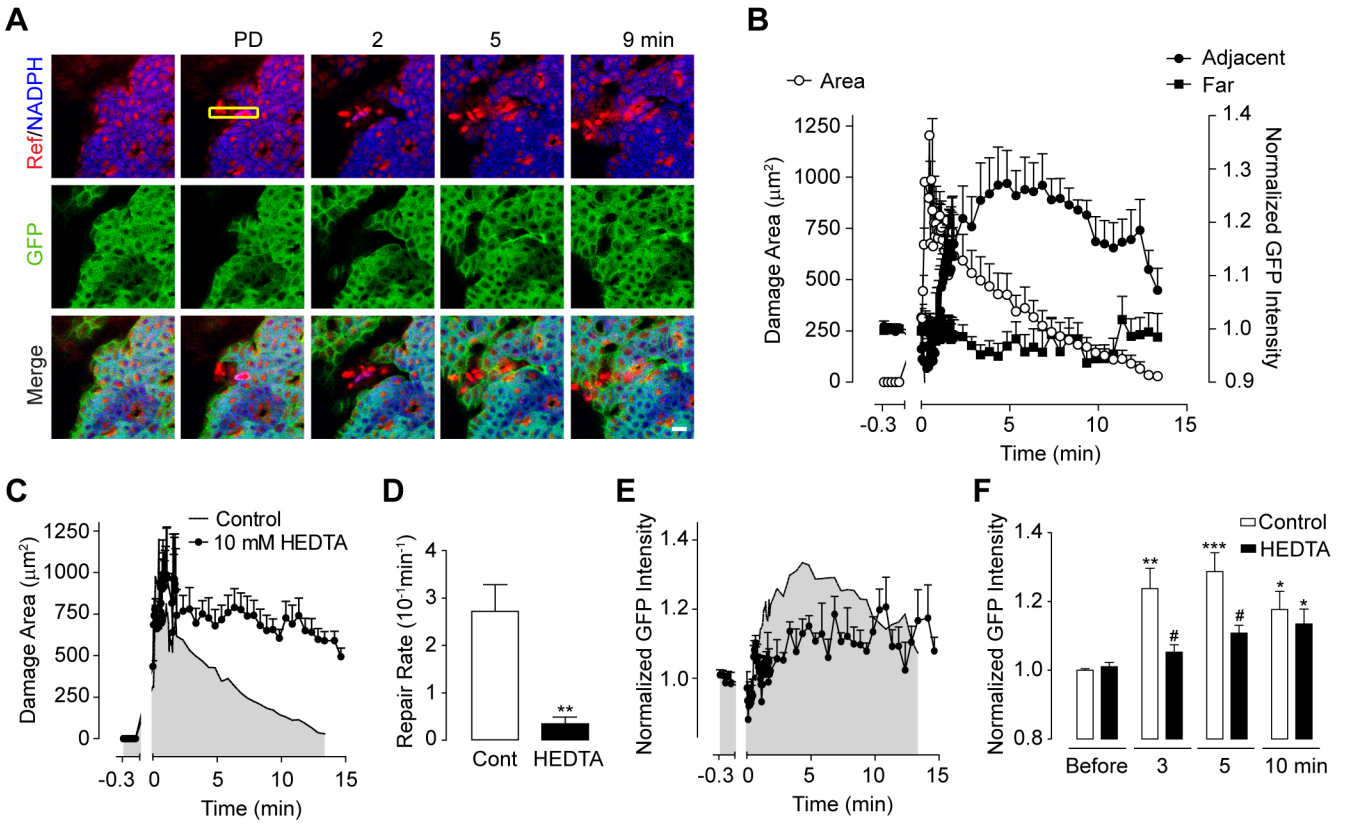

Fig. 1. Actin dynamics during restitution in mouse gastric epithelium *in vivo*. (A) Reflectance (Ref) and NAD(P)H (excitation 730 nm) or GFP (HuGE) images collected at the indicated times from a representative timecourse experiment in anesthetized mouse stomach. Gastric surface cells were photodamaged (PD) in the region marked by a yellow rectangle. Scale bar: 10 µm. (B) The damaged area was measured (left *y*-axis). GFP intensity was measured in viable cells adjacent to the damaged area or in viable cells >100 µm from damage area (adjacent and far; right *y*-axis). GFP intensity is normalized to the averaged resting value prior to damage. Mean±s.e.m., *n*=9. Experiment testing the effect of luminal perfusion of 10 mM HEDTA (*n*=5). Compiled results (mean±s.e.m.) showing (C) the timecourse of the amount of damaged area, which was used to derive the calculated repair rate (D). $^{**}P<0.01$ versus control (two-tailed *t*-test). Timecourse of GFP intensity (E) and values at specific indicated times (F). In C and E, control values were taken from B. $^{*}P<0.05$, $^{**}P<0.01$, $^{***}P<0.001$, versus prior to damage in the corresponding condition (one-way ANOVA with Dunnett's test). $^{\#}P<0.05$ versus control at corresponding time (two-tailed *t*-test).

(Fig. 2F). By integrating the observed properties, such as actin accumulation and dead cell motion, the model predicted these unobserved physical properties such as dead cell ejection velocity and the presence of actin-mediated force on the dead cell.

Furthermore, experimental data from individual cells suggest that the accumulation of actin is sustained even after the damaged area is closed (Fig. 2G). In order to explain this committed actin accumulation, we incorporated a phenomenological bi-stable switch (competition for actin monomers between two filamentous actin networks) (Byrne et al., 2016; Lomakin et al., 2015). This assumed switch predicts sustained actin accumulation after damage repair. The consistency between the temporal simulation and experimental observation suggests future areas to test the proposed mechanism versus the observed gastric epithelial repair.

Actin polymerization regulates paracellular permeability during gastric epithelial repair *in vitro*

F-actin stained by phalloidin was confirmed to increase in the lateral membrane next to the damaged area at ∼1 min after induction of cell damage (Fig. 2H). In this initial stage, ZO-1 remained at the apical pole and only subsequently moved toward the basal pole in a similar manner to that seen in the protrusions of migrating cells (Fig. 2H). These results suggest that in response to damage, actin accumulation precedes tight junction rearrangements.

We directly tested whether actin plays a role in regulating paracellular permeability during gastroid damage repair. Either Alexa 647 10K-dextran (molecular mass of 10,000 Da) or Lucifer Yellow (molecular mass of 444 Da) was added to the medium and paracellular leakage measured as the luminal accumulation of dye. We first used the same probes to track intracellular accumulation of the dyes after directed photodamage. 10K-dextran or Lucifer Yellow leaked negligibly into the dead cell unless damage was intentionally made to the basal plasma membrane (Fig. 3A; Fig. S5A). In response to basal damage, epithelial repair proceeds normally, but both 10K-dextran and Lucifer Yellow leak into the damaged cell immediately and then decrease over time (Fig. 3A; Fig. S5B,C). The time of fluorescence decrease is used to mark the time of the separation of the dying cell from the basolateral dye ocean, which can be visualized as being separated by GFP–actin at the basal membrane at about the 4 min time point (Fig. S5D). The repair is completed without adding a significant amount of dye leaking into the lumen (Fig. 3F). These results suggest that even with a compromised basolateral membrane, gastric repair can limit transcellular flux of material during repair of damage.

To investigate role of actin polymerization in the paired events of repair and paracellular permeability, we employed Cytochalasin D and Latrunculin A, both actin polymerization inhibitors, or Jasplakinolide, an actin stabilizer. In preliminary tests, these inhibitors increased paracellular leakage over time in normal

Journal of Cell Science (2018) 131, jcs216317. doi:10.1242/jcs.216317

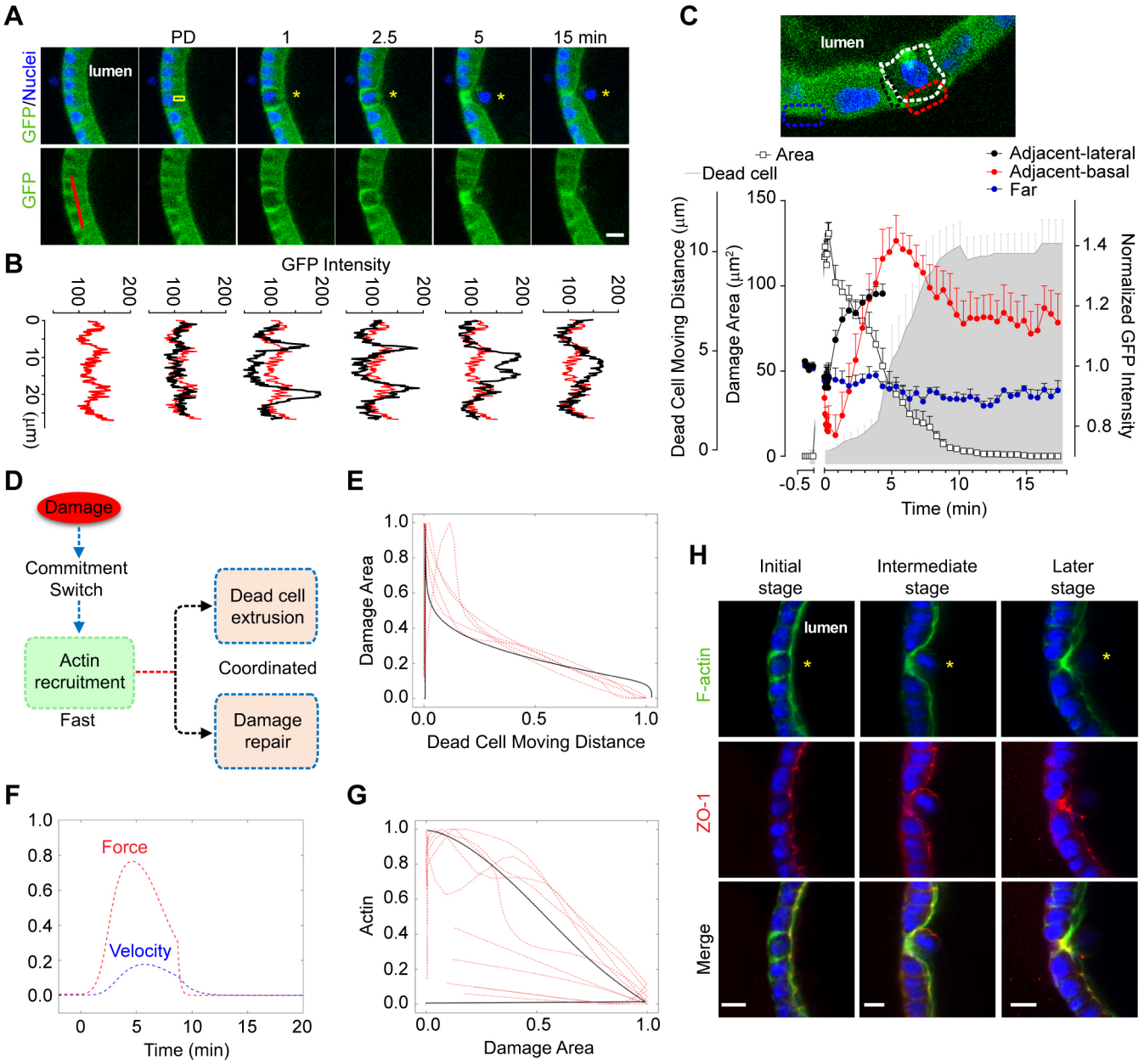

Fig. 2. Actin dynamics during restitution in mouse gastroids *in vitro*. (A) Nuclei (Hoechst 33342, excitation 730 nm) or GFP images collected at the indicated times from a representative timecourse experiment using a gastroid. A single gastric epithelial cell was photodamaged (PD) in the region marked by the yellow rectangle. Scale bar: 10 µm. (B) GFP fluorescence (average pixel intensity, arbitrary units) versus position was measured along the red line in A. Graphs display values prior to PD (red) in all graphs, versus the values at the indicated time point (black). (C) The damaged area (white dotted line) was measured. GFP intensity was measured in the lateral membrane (black) and basal compartment (red) of viable cells adjacent to the damaged area or in viable cells away from the damaged area (blue). GFP intensity is normalized to averaged resting value prior to damage. Mean±s.e.m., n=7. (D) The mathematical model diagram for dynamics of repair of damage. Nodes represent the model components; arrows indicate activation. (E) The damaged area (y-axis) shrinks before the extrusion of the dead cell (x-axis). The black curve indicates model simulation, and the red curves indicate data from individual cells. (F) Predicted velocity of the extruded cell (blue curve) and the force executed on the dead cell by the actin network of neighbor cells (red curve). (G) The sustained accumulation of actin even after the closure of the damaged area. The black curve indicates model simulation and the red curves indicate data from individual cells. (H) Immunofluorescence of F-actin and ZO-1 in PD gastroid epithelium. Gastroids were fixed with 4% PFA at 1, 3 and 8 min following PD. Gastroids were whole-mount stained for nuclei (Hoechst 33342, blue), F-actin (using Phalloidin, green) and ZO1 (tight junction, red). Scale bar: 10 µm. Yellow asterisks in A and H are the PD cell.

gastroids (Fig. S6A–C), suggesting that actin turnover is crucial for the maintenance of epithelial continuity. Cytochalasin D did not alter total cellular GFP intensity while Latrunculin A reduced it, but it is noted that over time Cytochalasin D led to clumping accumulation of GFP–actin over the entire cell (Fig. S6A–C), whereas Jasplakinolide caused GFP–actin accumulation specifically in the basal compartment and decreased GFP–actin in the cytosolic compartment (Fig. S6D,E). Results confirmed that the inhibitors were bioactive against actin in the gastroid with different mechanisms of action. After 1 h preincubation, all three inhibitors completely inhibited repair of damage and GFP–actin dynamics (Fig. 3A–E) and caused sustained paracellular leakage through the damaged area (Fig. 3F). These results suggest that actin assembly and/or disassembly is essential in repair.

Journal of Cell Science (2018) 131, jcs216317. doi:10.1242/jcs.216317

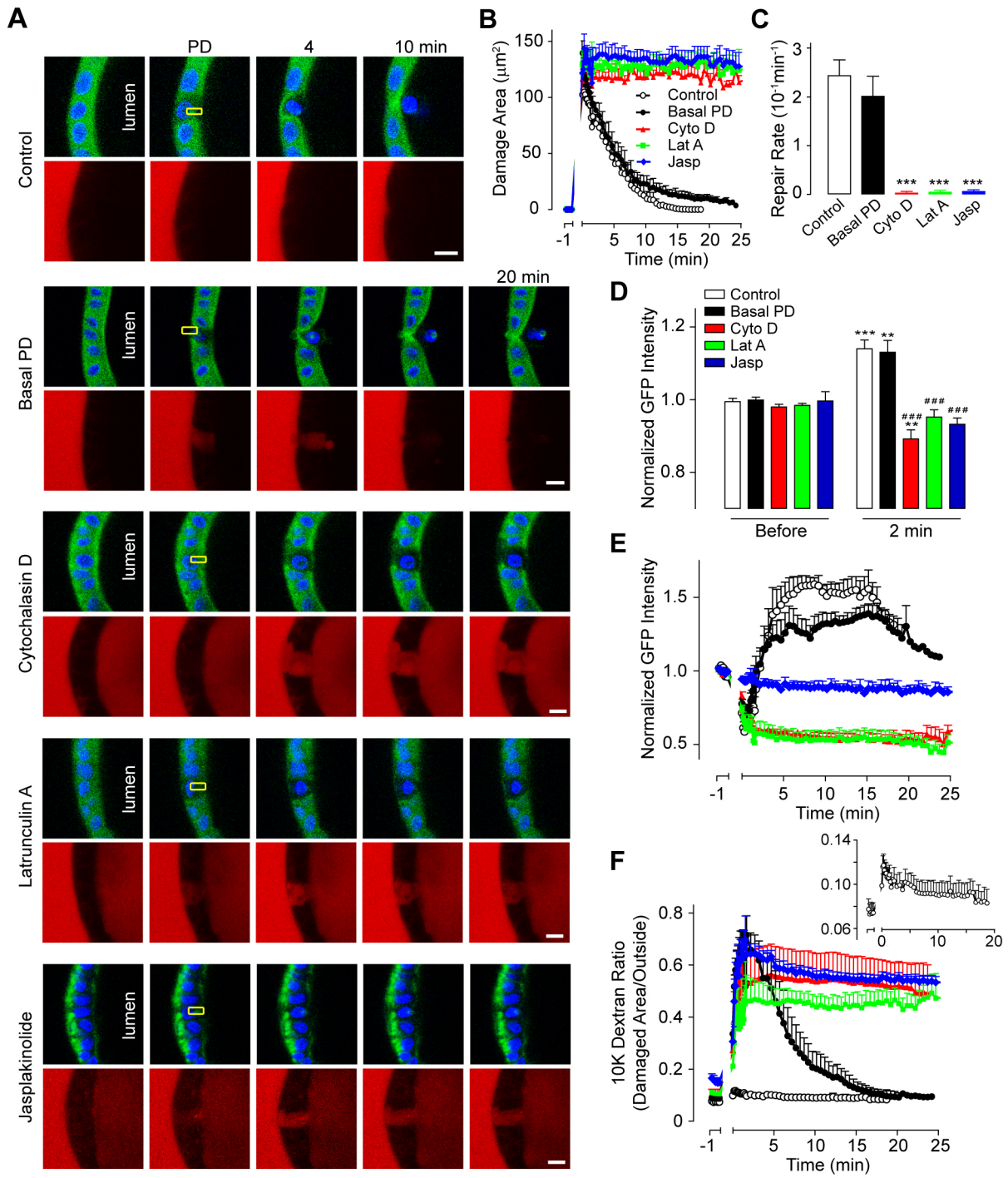

Fig. 3. Effect of actin inhibitors and paracellular leakage during the restitution in gastroids. (A) Nuclei (Hoechst 33342), GFP (HuGE) or Alexa Fluor 647-conjugated 10K-dextran (10 µM in the medium) images collected at the indicated times from a representative timecourse experiment using gastroids in the absence (control, *n*=7), or presence of Cytochalasin D (Cyto D; 1 µM, *n*=5), Latrunculin A (Lat A; 2 µM, *n*=6) or Jasplakinolide (Jasp; 1 µM, *n*=4) in the medium, or photodamage at the basal membrane (Basal PD; *n*=5). A single gastric epithelial cell was photodamaged (PD) in the region marked by yellow rectangle. Compiled results (mean±s.e.m.) showing timecourse of the amount of damaged area (B), which was used to derive the calculated repair rate (C). ***P<0.001 versus control (one-way ANOVA with Dunnett's test). Scale bar: 10 µm. (D) GFP intensity changes in the lateral membrane before and 2 min after PD. **P<0.01, ***P<0.001 versus prior to damage (two-tailed t-test). ###P<0.001 versus control at corresponding time (one-way ANOVA with Dunnett's test). (E) Timecourse of GFP intensity changes in the basal compartment of viable cells adjacent to the damaged area. GFP intensity is normalized to averaged resting value prior to damage. (F) Alexa Fluor 647-conjugated 10K-dextran intensity was measured in the damaged site and in the medium. Results (mean±s.e.m.) show the ratio of Alexa Fluor 647 intensity in damaged site to that in the medium (outside). The inset shows the expanded y-axis scale of the control group.

Since prolonged drug preincubation led to noticeable redistribution of cytosolic GFP–actin in Latrunculin A- or Jasplakinolide-treated conditions (Fig. S6), we performed photodamage experiments at earlier time points after treatment with Latrunculin A or Jasplakinolide to clarify the involvement of actin assembly or disassembly in the repair process. At 30 or 60 min preincubation,

Journal of Cell Science (2018) 131, jcs216317. doi:10.1242/jcs.216317

Latrunculin A significantly inhibited repair of damage and inhibited the increase of GFP–actin (Fig. S7A–C), without affecting the basal compartment of GFP–actin level (Fig. S7D), suggesting that F-actin filament elongation plays an important role. In contrast, Jasplakinolide did not inhibit repair of damage at early time points (Fig. S7E–G) when cytosolic actin was still available (Fig. S7H). These results demonstrate that actin assembly, but not actin disassembly, is essential to promote repair of damage.

To test whether specific mechanisms of actin assembly were required during repair, we examined the effect of CK-666 (an Arp2/3 inhibitor), and SMIFH2 (a formin inhibitor). CK-666 at a dose of 200 µM was shown to significantly inhibit repair of damage (Fig. 4A–C), and blocked an initial increase of GFP–actin in the lateral membrane in the migrating cell and delayed actin appearance in the basal compartment of the damaged area (Fig. 4D–F). This suggests that Arp2/3 is involved in the actin polymerization in response to damage. In contrast, SMIFH2 had no effect (Fig. 4). The effectiveness of both drugs was confirmed (positive control), as preincubation of CK-666 or SMIFH2 was shown to slow Jasplakinolide-induced GFP-actin accumulation in the basal compartment (Fig. S8), suggesting both inhibitors affect actin turnover in the gastroid.

Effect of known inhibitors of gastric restitution on actin dynamics *in vitro*

Similar to our *in vivo* study, addition of a Ca^{2+} chelator (EDTA) into the medium significantly inhibited both gastric repair of damage (Fig. 5A–C) and the increase in GFP–actin in a concentration-dependent manner (Fig. 5E–G). EDTA also inhibited dead cell exfoliation, seen as an impairment in movement of the dead cell into the lumen (Fig. 5D). It is noted that gastroids were often dissociated under 2 mM EDTA conditions, with increased GFP–actin in the cell membrane, suggesting that the cellular junction could not be maintained in the gastroids under very low Ca^{2+} conditions. Dissociated gastroids were not used for experiments/analysis. These findings suggest that extracellular Ca^{2+} plays an important role in increasing the initial actin polymerization and damage repair in gastroids.

We previously demonstrated *in vivo* that trefoil factor 2 (TFF2) and/or intracellular Ca^{2+} play an important role in the repair of damage, mediated by C-X-C chemokine receptor type 4 (CXCR4) (Aihara et al., 2013; Xue et al., 2010, 2011). Here, we test whether the CXCR4 inhibitor AMD3100 or the phospholipase C (PLC) inhibitor U73122 affects actin polymerization and repair of damage within the gastroid. Both AMD3100 and U73122 significantly slowed repair of damage and inhibited dead cell exfoliation (Fig. 5H–K), consistent with our

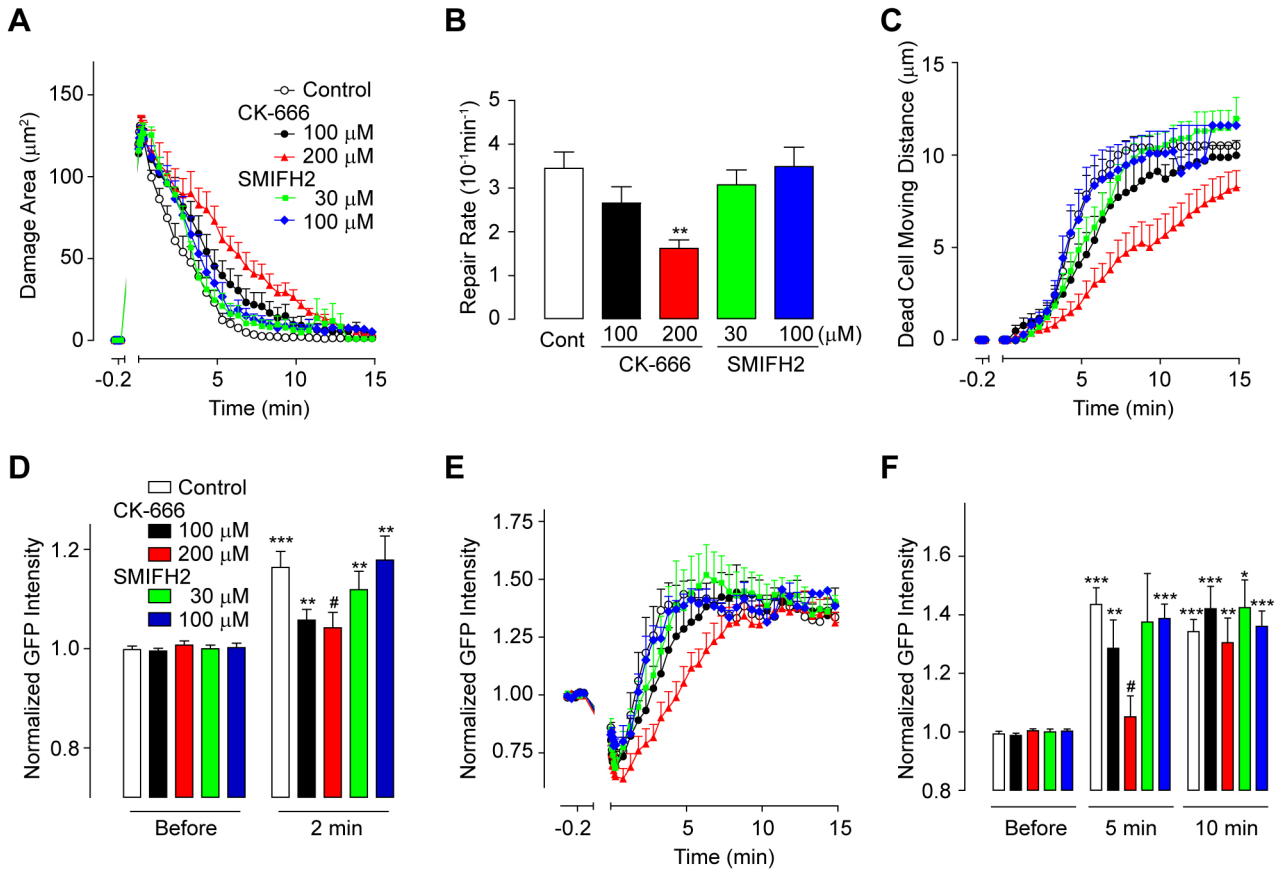

Fig. 4. Effects of Arp2/3 and formin inhibitors on restitution in gastroids. (A–C) Control (n=6), CK-666 (100 µM, n=10; 200 µM, n=8) or SMIFH2 (30 µM, n=6; 100 µM, n=5) was added to medium. Compiled results (mean±s.e.m.) showing timecourse of the amount of damaged area (A), which was used to derive the calculated repair rate (B) and dead cell moving distance (C). $^{**}P$<0.01, versus control (one-way ANOVA with Dunnett's test). (D) GFP intensity changes in the lateral membrane before and 2 min after PD. $^{**}P$<0.01, $^{***}P$<0.001 versus prior to damage (two-tailed t-test). $^{\#}P$<0.05 versus control at the corresponding time (one-way ANOVA with Dunnett's test). Timecourse of GFP intensity in the basal compartment of viable cells adjacent to the damaged area (E) and and values at specific indicated times (F). GFP intensity is normalized to averaged resting value prior to damage. $^{*}P$<0.05, $^{**}P$<0.01, $^{***}P$<0.001, versus prior to damage in corresponding conditions (one-way ANOVA with Dunnett's test). #, P<0.05 versus control at corresponding time (one-way ANOVA with Dunnett's test).

Journal of Cell Science (2018) 131, jcs216317. doi:10.1242/jcs.216317

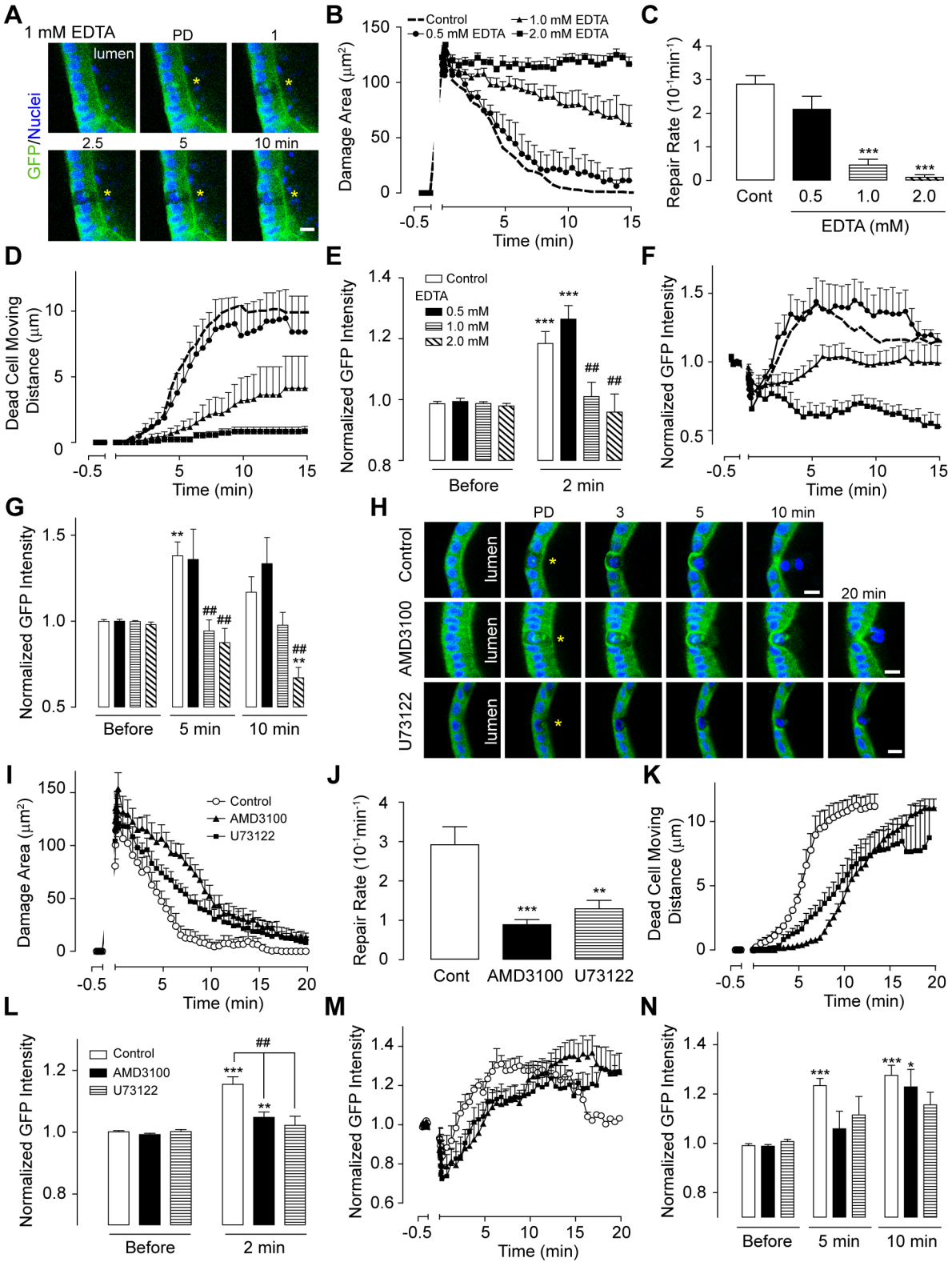

Fig. 5. See next page for legend.

previous findings *in vivo*. The drugs also slowed GFP–actin appearance at the lateral membrane in the migrating cell and basal compartment in the damaged area (Fig. 5L–N).

To test the role of myosin, the myosin light chain kinase (MLCK) classic inhibitor ML7, and the non-muscle myosin II inhibitor, (−)-Blebbistatin, were used. These drugs significantly inhibited repair of damage and slowed dead cell ejection (Fig. 6A–D). Both drugs significantly inhibited an initial increase of GFP–actin at the lateral membrane in the migrating cell and delayed actin appearance in the basal compartment in the damaged area (Fig. 6E–G). We also

Fig. 5. Effect of several inhibitors on restitution in gastroids. (A) Nuclei (Hoechst33342) or GFP (HuGE) images collected at the indicated times from a representative timecourse experiment using a gastroid in the presence of 1 mM EDTA in the medium. Scale bar: 10 µm. A single gastric epithelial cell was photodamaged (PD, yellow asterisk). Compiled results (mean±s.e.m.) with gastroids (control; n=7, 0.5 mM EDTA; n=5, 1 mM EDTA; n=8, 2 mM EDTA; n=6) showing timecourse of the amount of damaged area (B), which was used to derive the calculated repair rate (C) and dead cell moving distance (D). ***P<0.001 versus control (one-way ANOVA with Dunnett's test). (E) GFP intensity changes in the lateral membrane before and 2 min after PD. ***P<0.001 versus prior to damage (two-tailed t-test). ##P<0.01 versus control at corresponding time (one-way ANOVA with Dunnett's test). Timecourse of GFP intensity changes in the basal compartment of viable cells adjacent to the damaged area (F) and values at specific indicated times (G). GFP intensity is normalized to the averaged resting value prior to damage, and data show mean ±s.e.m. **P<0.01 versus prior to damage in corresponding conditions (one-way ANOVA with Dunnett's test). ##P<0.01 versus control at the corresponding time (one-way ANOVA with Dunnett's test). Control values were taken from Fig. 2C. (H) Representative timecourse images of control (n=5), and AMD3100-treated (CXCR4 inhibitor, 1 µM, n=5) or U73122-treated (PLC inhibitor, 10 µM; n=5) gastroids. The yellow asterisk indicates the PD cell. Scale bar: 10 µm. Compiled results (mean±s.e.m.) showing timecourse of the amount of damaged area (I), which was used to derive the calculated repair rate (J) and dead cell moving distance (K). **P<0.01, ***P<0.001 versus control (one-way ANOVA with Dunnett's test). (L) GFP intensity changes in the lateral membrane. **P<0.01, ***P<0.001 versus prior to damage (two-tailed t-test). ##P<0.01 versus control at corresponding time (one-way ANOVA with Dunnett's test). Timecourse of GFP intensity in the basal compartment of viable cells adjacent to the damaged area (M) and values at specific indicated times (N). GFP intensity is normalized to the averaged resting value prior to damage. *P<0.05, ***P<0.001 versus prior to damage in corresponding conditions (one-way ANOVA with Dunnett's test).

confirmed that (+)-Blebbistatin, the inactive enantiomer of (−)-Blebbistatin, had no effect on these processes (Fig. 6). These results suggest that cell membrane contraction partially contributes to GFP–actin accumulation and is crucial for dead cell exfoliation.

We further investigated effects of Rac1 (NSC23766), FAK (PF-562271), Cdc42 (ML141) or ROCK (Y27632) inhibitors on repair of damage. NSC23766 significantly accelerated repair, while ML141 and PF-562271 had negligible effects on the repair rate, but they appeared to slow the process of exfoliation in the later phase (Fig. 7). In these cases, actin polymerization still occurred with these drug treatments, with no consistent pattern of inhibition or stimulation of actin dynamics with these measurements. In contrast, Y237632 significantly inhibited repair and partially blocked actin dynamics (Fig. 7).

Since ROCK is a downstream effector of RhoA, we tested whether C3 transferase (CT04) inhibits the repair and actin dynamics. Gastroids treated with C3 transferase for 4 h showed normal morphology and actin distribution at concentrations up to 10 µg/ml (Fig. 8A). Treatment of C3 transferase (10 µg/ml) significantly inhibited repair (Fig. 8B–D) and the initial increase of GFP–actin at the lateral membrane in the migrating cell, and delayed the appearance of actin in the basal compartment in the damaged area (Fig. 8E–G).

DISCUSSION

Epithelial restitution is defined by a rapid cell migration to restore continuity of epithelium within minutes to hours without cellular proliferation (Aihara and Montrose, 2014; Critchlow et al., 1985; Yanaka et al., 2002). Herein, we showed that gastroids allow us to evaluate cell migration, dead cell extrusion and actin cytoskeletal dynamics using fluorescent probes in real time. We also clearly demonstrated in real-time that actin increased locally in the lateral membrane adjacent to a damaged site within ∼1 min after damage, and that this accumulation then extended to the basal site of damaged area. This quick repair of damage in the gastroid is similar to purse-string wound closure, which is observed in a sheet of Caco-2 or MDCK cells, which are polarized epithelial cell lines (Kuipers et al., 2014; Russo et al., 2005; Tamada et al., 2007). Importantly in the present study, we find that actin dynamics during natural cell shedding processes mimics that of photodamage-induced repair in the gastroid and we observed a quick increase of actin in the leading edge in response to relatively larger damage *in vivo*. We did not observe any cell division during the repair of damage that occurred over 10–15 min, suggesting that our gastroid model *in vitro* is mediated by restitution and mimics the *in vivo* process.

After the cell is injured and the damaged area generated, the actin network quickly assembles and leads to cell migration into the damaged area, which results in fast shrinkage of the damaged area as well as dead cell exfoliation. The order of this event sequence is identical to previous observations in MDCK cells or in the *Drosophila* damage model induced by laser ablation (Abreu-Blanco et al., 2011; Kuipers et al., 2014; Tamada et al., 2007), but our system was able to trace dead cell movement to directly analyze coordination with actin and the wounded area. Active protrusion of the cells, while being in physical contact with the dead cell, results from a physical force that causes the extrusion of the dead cell. After the dead cell moves sufficiently far away, the force from actin is no longer experienced and the dead cell then stops moving due to the resistance from the environment. Meanwhile, the actin network also mediates the migration of the neighbor healthy cells into the blank area left by the extruded dead cell. Thus, a coherent feedforward loop, in which the actin network is upstream of both processes, can facilitate their proper coordination. Furthermore, the extrusion of the dead cell follows the actin network assembly after a time delay of ∼5 min. This time delay allows the dead cell to serve as a temporary 'kitchen plug' and reduces the leakage caused by cell death.

It has been reported that the dead cell is immediately permeabilized following two-photon laser ablation in MDCK cell (Kuipers et al., 2014). In the present study, interestingly, leakage of Lucifer Yellow or 10K-dextran into the damaged cell is negligible when damage is made in the center of the cell, while damage induced to the basal membrane caused Lucifer Yellow or 10K-dextran to penetrate the damaged cell in the gastroid. With either damage site, regions of the plasma membrane remain impermeable until the damaged cell is isolated from the monolayer by migrating cells. In fact, we observed that fluorescent dyes in the dead cell started diffusing into the lumen once the basal domain was sealed from the monolayer. We previously demonstrated that fluorescent dextrans (intravenous treatment) accumulated in the photodamaged cells *in vivo* but did not leak out into lumen (Demitrack et al., 2010). Thus, data suggest that even dead cells sustain a certain degree of barrier function to hold separation between the lumen and serosal sides.

The inhibition of actin polymerization deters gastric wound healing (Banan et al., 1996; Critchlow et al., 1985; Paehler Vor der Nolte et al., 2017; Watanabe et al., 1994a). Consistent with these findings, we also observed that inhibition of actin dynamics completely hindered initiation of cell migration as well as dead cell exfoliation. In the present study, we used three different actin inhibitors that inhibit actin by different mechanisms as schematically summarized by Peng et al. (2011). Cytochalasin D, which binds barded ends of F-actin filaments to inhibit actin assembly (Cooper, 1987; Peng et al., 2011), and is also reported to slow disassembly of F-actin in mammalian cells (Kueh et al., 2008),

Journal of Cell Science (2018) 131, jcs216317. doi:10.1242/jcs.216317

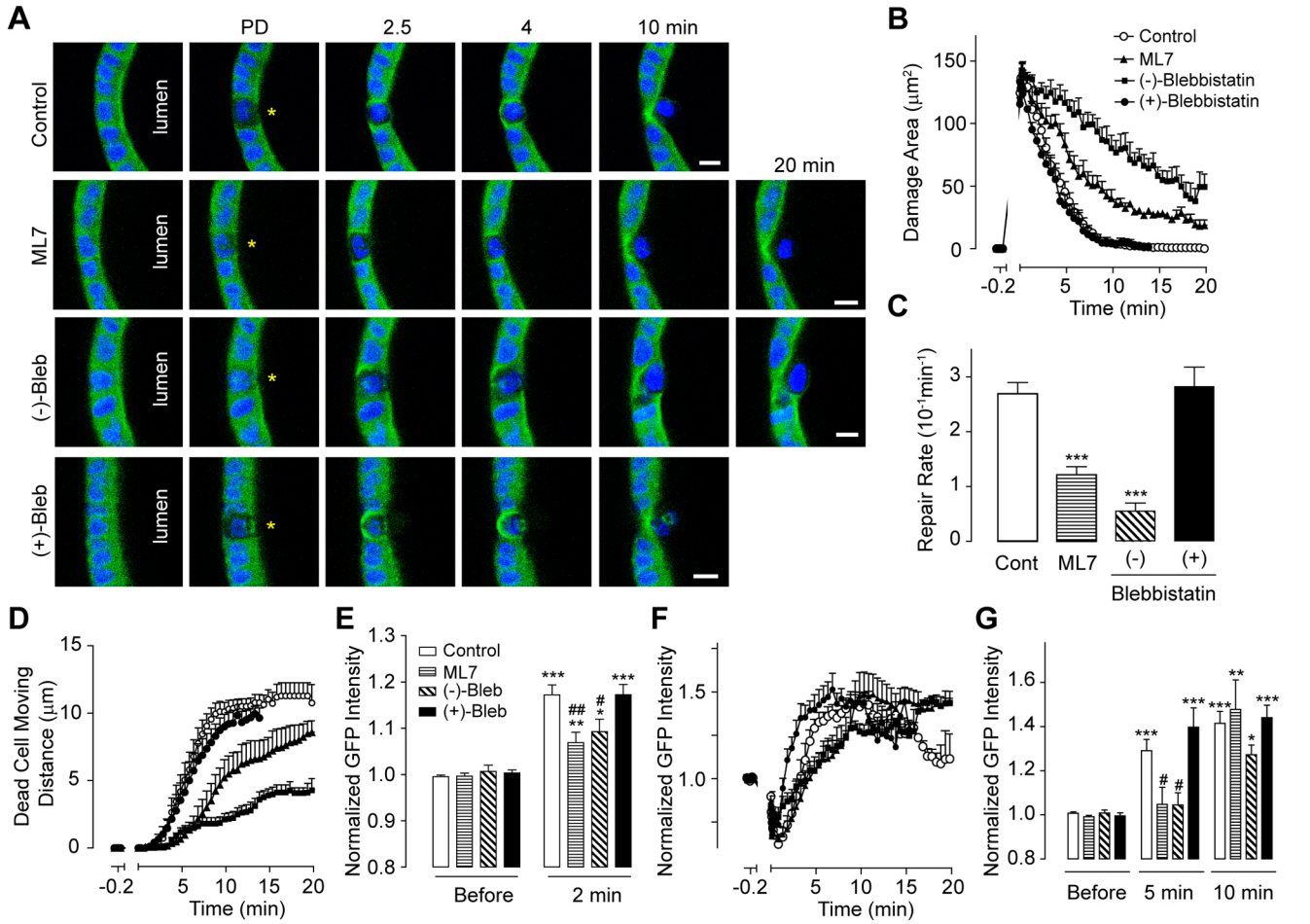

Fig. 6. Effects of MLCK and myosin II inhibitors on restitution in gastroids. (A) Nuclei (Hoechst33342) or GFP (HuGE) images collected at the indicated times from a representative timecourse experiment using gastroids. Scale bar: 10 µm. A single gastric epithelial cell was photodamaged (PD, yellow asterisk). Control (n=9), ML7 (10 µM, n=5), (−)-Blebbistatin [(−)-Bleb; 50 µM, DMSO 0.25%, n=5] or (+)-Blebbistatin [(+)-Bleb, 50 µM; DMSO 0.25%, n=6] was added to medium. Compiled results (mean±s.e.m.) showing timecourse of the amount of damaged area (B), which was used to derive the calculated repair rate (C) and dead cell moving distance (D). ***P<0.001 versus control (one-way ANOVA with Dunnett's test). (E) GFP intensity changes in the lateral membrane before and 2 min after PD. *P<0.05, **P<0.01, ***P<0.001 versus prior to damage (two-tailed t-test). $^{\#}P$<0.05, $^{\#\#}P$<0.01 versus control at corresponding time (one-way ANOVA with Dunnett's test). Timecourse of GFP intensity in the basal compartment of viable cells adjacent to the damaged area (F) and values at specific indicated times (G). GFP intensity is normalized to averaged resting value prior to damage. *P<0.05, **P<0.01, ***P<0.001, versus prior to damage in corresponding conditions (one-way ANOVA with Dunnett's test). $^{\#}P$<0.05 versus control at corresponding time (one-way ANOVA with Dunnett's test).

inhibited repair, suggesting that action of actin assembly or disassembly is crucial in epithelial repair. Latrunculin A directly binds actin monomers (G-actin) to prevent actin polymerization and facilitates actin disassembly (Peng et al., 2011; Spector et al., 1983), whereas Jasplakinolide stabilizes F-actin filaments resulting in inhibition of disassembly, and also promotes actin polymerization (Peng et al., 2011). In the present study, Latrunculin A completely inhibited repair, while short-term treatment with Jasplakinolide did not inhibit repair. The Arp2/3 complex and formins are accessory proteins involved in actin polymerization; the former promotes formation of actin branches and is active in lamellipodia to produce force, while the latter stimulates unbranched actin filament formation (Bieling et al., 2016; Mueller et al., 2017; Pollard, 2007). Our study indicates that the increase of actin in the lateral membrane is mediated by activation of Arp2/3, but not formins. Taken together, results clearly demonstrate that actin polymerization, and branching in the existing actin filaments, initiates the process of epithelial repair of damage.

MLC phosphorylation mediated by MLCK, which is activated by the intracellular Ca^{2+} and calmodulin complex, acts to stimulate myosin II, resulting in a facilitation of cell contraction (Bement et al., 1993; Kuipers et al., 2014; Russo et al., 2005; Tamada et al., 2007). In rabbit gastric epithelial cells, inhibition of either the Ca^{2+}/calmodulin complex or MLCK prevented cell migration (Ranta-Knuuttila et al., 2002; Watanabe et al., 1994b). In the present study, MLCK or non-muscle myosin II inhibition partially reduced the initial GFP–actin increase at the lateral membrane in the migrating cell, suggesting that membrane contraction partially contributes to increased GFP–actin fluorescence intensity at the lateral membrane. These inhibitors also slowed cell protrusion and inhibited restitution. These results suggest that MLCK or non-muscle myosin II are not involved in the processes that lead to actin polymerization after damage, but instead is engaged with actin in gastric epithelial cell protrusion as well as contraction.

We previously reported that extracellular Ca^{2+} plays an important role in restitution *in vivo* (Aihara et al., 2013). Both *in vivo* and *in vitro*, extracellular Ca^{2+} chelation inhibited actin dynamics and inhibited repair in this study. Ca^{2+} has been shown to be involved in maintaining adherens and tight junctions (Gonzalez-Mariscal et al., 1990; Marchiando et al., 2011), so it was not surprising that high

Journal of Cell Science (2018) 131, jcs216317. doi:10.1242/jcs.216317

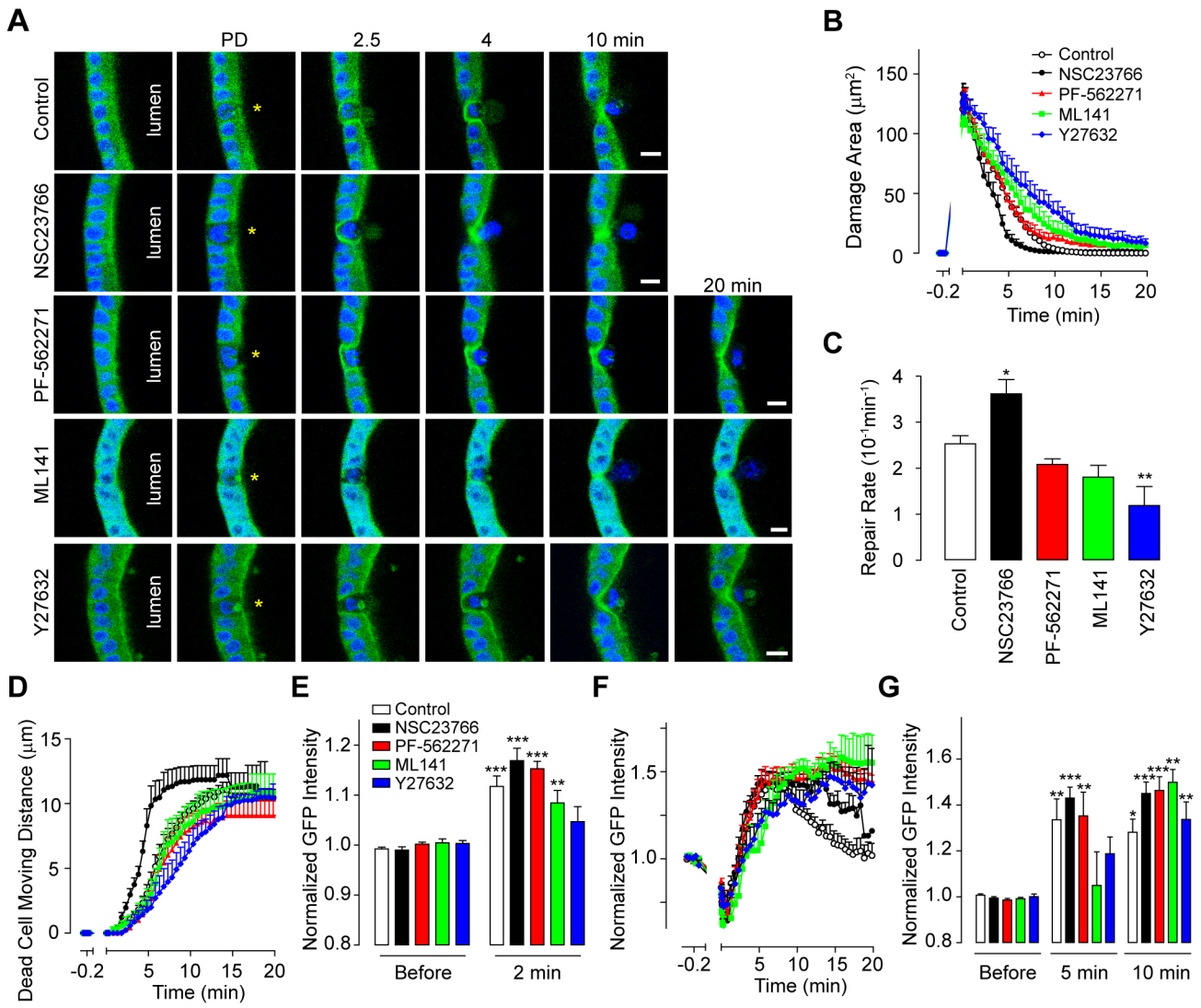

Fig. 7. Effects of several inhibitors on restitution in gastroids. (A) Nuclei (Hoechst 33342) or GFP (HuGE) images collected at the indicated times from a representative timecourse experiment using gastroids. Scale bar: 10 µm. A single gastric epithelial cell was photodamaged (PD, yellow asterisk). Control (n=11), NSC23766 (Rac1 inhibitor, 50 µM, n=6), PF-562271 (FAK inhibitor, 1 µM, n=6), ML141 (Cdc42 inhibitor, 20 µM, n=5) or Y27632 (ROCK inhibitor, 20 µM, n=6) was added to medium. Compiled results (mean±s.e.m.) showing timecourse (B), which was used to derive the calculated repair rate (C) and dead cell moving distance (D). *P<0.05, **P<0.01 versus control (one-way ANOVA with Dunnett's test). (E) GFP intensity changes in the lateral membrane before and 2 min after PD. **P<0.01, ***P<0.001 versus prior to damage (two-tailed t-test). Timecourse of GFP intensity in the basal compartment of viable cells adjacent to the damaged area (F) and values at specific indicated times (G). GFP intensity is normalized to averaged resting value prior to damage. *P<0.05, **P<0.01, ***P<0.001, versus prior to damage in corresponding conditions (one-way ANOVA with Dunnett's test).

concentrations of EDTA caused cell dissociation within the gastroid. Additionally, inhibitors of actin dynamics increased paracellular leakage of 10K-dextran into otherwise unperturbed gastroids. This suggests that extracellular Ca^{2+} is an essential factor to regulate actin dynamics, and maintains transepithelial permeability as well as cellular motility. In the gastroid model, a dead cell generally extrudes into the luminal side, even if damage is induced onto the basal membrane. Moreover, actin always increases at the membrane adjacent to the damaged site. We speculate that Ca^{2+} dynamics at the damage site regulate actin assembly at the lateral membrane, potentially via the dead cell providing the necessary signal to initiate a repair program and communicating to neighboring cells through cell–cell adhesion contacts (Gagliardi et al., 2018; Lubkov and Bar-Sagi, 2014; Monier et al., 2015). In particular, it has been proposed that E-cadherin anchors actomyosin to generate the force to extrude dead cells (Abreu-Blanco et al., 2011; Lecuit and Yap, 2015; Michael et al., 2016). It has also been reported that intracellular Ca^{2+} increases in the neighboring cells in response to damage as well as playing an important role in the repair of damage (Aihara et al., 2013; Antunes et al., 2013; Hunter et al., 2015). Elegant studies have shown that this intracellular Ca^{2+} action is required for E-cadherin redistribution at the wounded junction and Ca^{2+} influx mediated by TRPM channels immediately occurs after wounding and coordinates actomyosin flow (Antunes et al., 2013; Hunter et al., 2015). Our work identifies specific cellular sites for study, but additional methodologies will be needed to identify the role and interactions among such factors within this repair microenvironment.

Our work shows that the physiological triggers of gastric epithelial repair *in vivo* are preserved in the organoid model, and are therefore intrinsic to the epithelial layer. TFF2 and CXCR4

Journal of Cell Science (2018) 131, jcs216317. doi:10.1242/jcs.216317

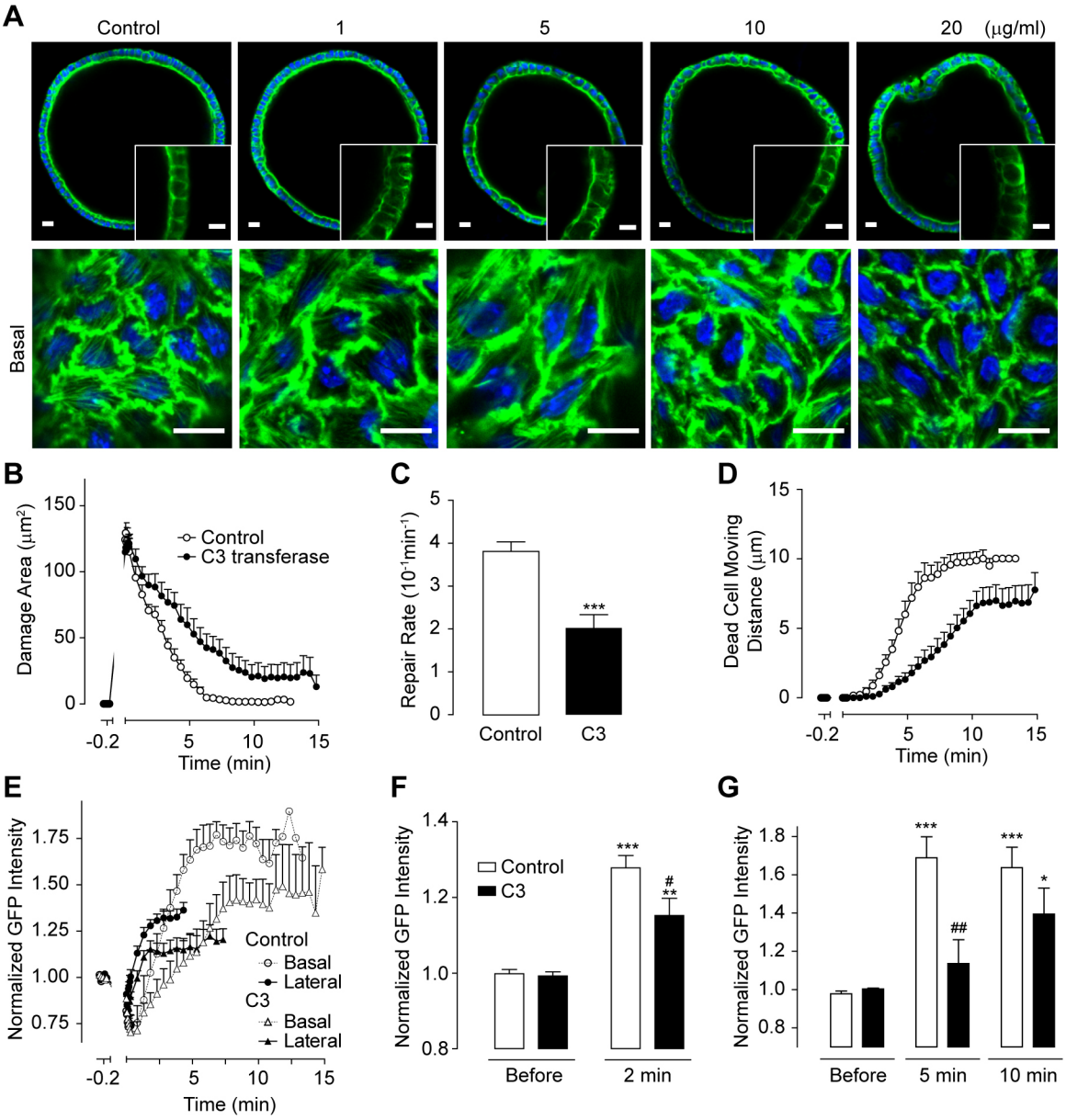

Fig. 8. Effect of RhoA inhibitor on restitution in gastroids. (A) Gastroids were incubated with C3 transferase at an indicated concentration for 4 h and fixed with 4% PFA. Representative images show nuclei (Hoechst 33342, blue) and F-actin (using phalloidin, green). Scale bars: 10 µm. A single gastric epithelial cell was photodamaged in the absence (control; sterile water, *n*=7) or the presence of C3 transferase (C3; 10 µg/ml, *n*=7). Compiled results (mean±s.e.m.) showing the timecourse of the amount of damaged area (B), which was used to derive the calculated repair rate (C) and dead cell moving distance (D). ***P<0.001 versus control (two-tailed *t*-test). Timecourse of GFP intensity in the lateral and basal compartment of viable cells adjacent to the damaged area (E) and values at specific indicated times (F, lateral; G, basal). GFP intensity is normalized to the averaged resting value prior to damage. In F, **P<0.01, ***P<0.001 versus prior to damage in corresponding conditions (two-tailed *t*-test). $^{\#}P$<0.05 versus control at corresponding time (two-tailed *t*-test). G: *P<0.05, ***P<0.001 versus prior to damage (two-tailed *t*-test). $^{\#\#}P$<0.01 versus control at corresponding time (two-tailed *t*-test).

promote gastric restitution *in vivo* (Aihara et al., 2017; Xue et al., 2010, 2011). We confirmed that CXCR4 inhibitor slowed repair in gastroids. It is reported that the activation of CXCR4 in the Caco-2 cells increases the intracellular Ca^{2+} concentration, resulting in enhancing intestinal epithelial restitution through reorganization of the actin cytoskeleton (Agle et al., 2010). It also is reported that exogenous TFF3 limits disruption to the F-actin in Caco-2 cells (Xu et al., 2011). In the present study, PLC inhibitor also inhibited repair of damage in the gastroids, consistent with previous *in vivo* and *in vitro* studies (Aihara et al., 2013; Watanabe et al., 1994a). Inhibition of PLC or CXCR4 strongly prevented an initial increase of GFP–actin in the lateral membrane in the migrating cell, suggesting that intracellular Ca^{2+} plays important role to initiate actin dynamics and TFF2 functions as an upstream effector in response to gastric epithelial damage. Thus TFF2 and CXCR4 signaling may also affect actin dynamics via regulating cell protrusion and contraction, and that this action might be mediated by Ca^{2+} mobilization. It is also possible that TFF2 signaling affects myosin dynamics, but this will require further studies.

Rho/ROCK signaling is known to regulate cell migration (Hall, 1998; Matsuoka and Yashiro, 2014; Mitra et al., 2005; Zhao and Guan, 2011). Additionally, gastric mucosal injury induces FAK

Journal of Cell Science (2018) 131, jcs216317. doi:10.1242/jcs.216317

phosphorylation, and others have observed that indomethacin (which slows gastric repair) reduced FAK immunoreactivity in the migrating cell after NaCl-induced gastric injury (Szabó et al., 2002). We observed that inhibitors for Cdc42 or FAK appeared to inhibit restoration of normal actin levels following the completion of repair; however, they did not affect the total repair rate or dead cell exfoliation rate. It is reported that ROCK is critical for actin assembly and actomyosin activity in the purse-string wound closure model (Abreu-Blanco et al., 2011; Antunes et al., 2013; Russo et al., 2005). Consistent with these studies, we observed that ROCK inhibition prevented actin dynamics and delayed restitution. It is reported that RhoA, which acts upstream of ROCK, stimulates the initial events of protrusion (Machacek et al., 2009). Similar to what was seen upon ROCK inhibition, we demonstrated that RhoA inhibition blocked actin dynamics as well as restitution. RhoA/ROCK regulates myosin II to control contraction, whereas RhoA also regulates formins to promote unbranched actin nucleation (Goode and Eck, 2007; Pellegrin and Mellor, 2007). It has been shown that silencing Dia, which acts downstream of RhoA, inhibited wound repair in *Drosophila*, which suggests that a formin, but not the Arp2/3 complex, is the main regulator of actin polymerization within their system (Antunes et al., 2013). We could not confirm the involvement of formins in the pharmacological approach we used in the gastric restitution, but our results suggest that RhoA/ROCK likely stimulates cell contraction and protrusion in response to damage. Thus, it is possible that the Cdc42 and FAK primarily regulate the later phase of the gastric repair process and RhoA/ROCK is mainly involved in initial cell stretching and generation of force to extrude the dead cell, but not actin polymerization.

Since the sustained actin accumulation after the decrease of damage area was observed, a bistable ‘commitment switch’ was assumed. The molecular network underlying the commitment switch for actin dynamics remains largely unknown in normal epithelial cells, although multiple positive feedbacks have been proposed in other models. It has been reported that actin protrusion is promoted by Rac1, and that the activity of Rac1 is regulated by a mutually antagonistic positive feedback between Rac1 and RhoA (Byrne et al., 2016; Lomakin et al., 2015). Early studies have observed that both RhoA and Rac1 are strongly expressed during wound healing in RGM1 cells (Osada et al., 1999). In the present study, inhibition of Rac1 promoted restitution in gastroids. Rac1 promotes intestinal epithelial cell migration after wounding (Rao et al., 2008). It is reported that Rac1 has either inhibitory or stimulatory effects on cell migration depending on types of cell line, and this stimulation upon Rac1 inhibition was accompanied with the enhancement of RhoA activity (Zuo et al., 2006). It is possible that Rac1 inhibition results in an increase of RhoA activity in the gastroids. Two redundant positive-feedback mechanisms between RhoA, ROCK, and non-muscle myosin II have also been proposed to function as a bistable switch (Priya et al., 2015). Furthermore, a biomechanical positive feedback has been proposed to amplify the recruitment of essential molecules including myosin II (Munjal et al., 2015). In our work, inhibition of RhoA, ROCK and myosin II all partially inhibited actin dynamics, consistent with their positive contribution to a proposed commitment switch. We have not systemically identified the precise molecular pathway of this commitment switch. Further studies will be necessary to reveal the molecular composition of the switch.

In conclusion, gastric organoids are a useful system to augment studies of epithelial repair in native tissue. Our studies in this system have shown that actin dynamics regulated by Ca^{2+} signaling and the physiological effector TFF2/CXCR4 initiate gastric repair of damage, followed by the promotion of cell migration to complete restitution. These actin dynamics are tightly correlated with dead cell exfoliation and are associated with force generation. This organoid model will provide new insight into the molecular and cellular mechanisms of gastric epithelial restitution by enabling experimental approaches and therapeutic validations that cannot currently be performed in either animal or native human tissues.

MATERIALS AND METHODS

Animal husbandry and surgery

Experiments used HuGE heterozygous mice or HuGE negative mice from same colony (Gurniak and Witke, 2007). Animals were fed a standard rodent chow diet, and had free access to water. HuGE mice used in the experiments carried one GFP–actin knock-in allele in the profilin 1 locus (Gurniak and Witke, 2007), and they were confirmed by PCR genotyping. Male and female mice were used for experimentation at 2–4 months of age. All animal procedures were approved by the Institutional Animal Care and Use Committee of the University of Cincinnati.

The surgical preparation of animals has been described previously (Aihara et al., 2014, 2013; Xue et al., 2010). Mice were anesthetized with inactin (10 mg/kg body weight, intraperitoneal) and ketamine (50 mg/kg body weight, intraperitoneal), and the exposed gastric mucosa protruded into a perfusion chamber on the stage of an inverted confocal and two-photon microscope (Zeiss LSM 510 NLO), with the microscope stage enclosed and heated to keep the body temperature of the animal at ∼37°C.

Generation of gastroids

Gastroids from mouse gastric corpus were generated as described previously (Mahe et al., 2013; Schumacher et al., 2015a). Briefly, isolated mouse gastric corpus was incubated with rocking at 4°C for 2 h in 10 mM EDTA in Dulbecco’s phosphate-buffered saline (DPBS) without Ca^{2+} and Mg^{2+}. Then tissue was placed into ice-cold dissociation buffer (43.3 mM sucrose and 54.9 mM D-sorbitol, Sigma, in DPBS) and shaken forcefully by hand to dissociate individual glands. Dissociated glands were centrifuged at 150 ***g*** for 5 min at 4°C, and the pellet re-suspended in Matrigel. Suspended glands in Matrigel were added to an eight-well Lab-Tek chamber with coverglass (Thermo Scientific). After Matrigel polymerization at 37°C, advanced DMEM/F12 supplemented with 2 mM GlutaMax, 10 mM HEPES, 100 U/ml penicillin/100 µg/ml streptomycin, 1× N2 and 1× B27 supplements (Life Technologies), Wnt3a-conditioned medium (50%), R-spondin-conditioned medium (10%), Noggin-conditioned medium (10%), [Leu15]-Gastrin I (10 nM, Sigma) and EGF (50 ng/ml, PeproTech) was added to the wells and replaced every 4 days. Gastroids were cultured in a 5% CO_2 incubator at 37°C.

Induction of two-photon laser-induced microlesion

In vivo animal

Tissue NAD(P)H autofluorescence (Ti-Sa laser, excitation of 730 nm, emission of 435–485 nm) and GFP–actin fluorescence (excitation of 488 nm, emission of 500–550 nm) in the gastric corpus were collected simultaneously using a C-Apochromat 40× objective with a confocal reflectance image (reflecting 730 nm light to show cell/tissue structure). Gastric epithelial damage was induced by a two-photon laser (photodamage) as described previously (Aihara et al., 2014, 2013; Xue et al., 2010). After collecting a set of control images, a small rectangle region (≈200 µm^2) of gastric surface epithelium in the corpus was repetitively scanned at high Ti-Sa laser power (350 mW average) for 150 iterations. The mucosal surface was exposed to pH 5 solution (150 mM NaCl and 4 mM homopipes; Research Organics). In some experiments, solutions contained 10 mM HEDTA (Fluka).

In vitro gastroid

Experiments were performed in organoid culture medium under 5% CO_2 at 37°C (incubation chamber, PeCon, Erbach, Germany) on an inverted confocal microscope (Zeiss LSM 510 NLO) and imaged with a C-Achrophan NIR 40× objective. The gastroid was preincubated with

Hoechst 33342 (10 µg/ml, Thermo Fisher Scientific) for 30 min to visualize nuclei. Images of Hoechst 33342 (Ti-Sa laser, excitation of 730 nm, emission of 435–485 nm) and GFP–actin (excitation 488 nm, emission 500–550 nm) in the gastroid were collected simultaneously with a transmitted light. In some cases, Alexa Fluor 647-conjugated 10K-dextran (10 µM, excitation 633 nm, emission 650–700 nm, Thermo Fisher Scientific) was added to the medium of the HuGE gastroids while Alexa Fluor 647-conjugated 10K-dextran and Lucifer Yellow (20 µM, excitation 458 nm, emission 500–550 nm, Molecular Proves) were added to the medium of the HuGE-negative gastroids. After collecting a set of control images, a small rectangle region (≈5 μm^2) of a single cell was repetitively scanned at high Ti-Sa laser power (730 nm; 650 mW average) for 500 iterations (duration, 2–3 s). Gastroids locating ∼150–300 µm from the cover glass in the Matrigel were used. In some cases, EDTA (0.5–2 mM) was applied to medium. Unless noted, gastroids were preincubated at least 1 h prior to experiments with the following drugs, which were kept in the medium during experiments; Cytochalasin D (1 µM, Sigma), Latrunculin A (2 µM, Sigma), Jasplakinolide (1 µM, Cayman), AMD3100 (1 µM, Sigma), U73122 (10 µM, Enzo life sciences), ML7 (10 µM, Calbiochem), (−)-Blebbistatin (50 µM, Sigma), (+)-Blebbistatin (50 µM, Sigma), NSC23766 (50 µM, Cayman), PF-562271 (1 µM, a gift from Dr James E. Casanova, Virginia University, VA), ML141 (20 µM, Calbiochem), Y27632 (20 µM, Enzo life sciences), CK-666 (100-200 µM, Sigma), and SIMFH2 (30-100 µM, Sigma). C3 transferase (CT04, 1-20 µg/ml, Cytoskeleton) was applied to medium 4 h prior to experiments. Final DMSO concentration was <0.2% in the medium, equal amount of DMSO was added to medium in control group unless stated.

The damage–repair cycle was measured independently several times per animal in different locations of the corpus, or once per gastroid, and outcomes from at least three animals or four different gastroids, were compiled for each experimental protocol. In one set of experiments, shown in Fig. S2, two damage cycles were imposed on gastroids.

Long-term live imaging of gastroids

Live imaging were performed in organoid culture medium under 5% CO_2 and at 37°C (incubation chamber, PeCon, Erbach, Germany) on an inverted confocal microscope (Zeiss LSM 710 NLO) and imaged with a Plan-Apochromat 20× objective. GFP–actin (excitation 488 nm, emission 500–550 nm) florescence from the gastroids were collected. In some cases, Alexa Fluor 647-conjugated 10K-dextran (10 µM, excitation 633 nm, emission 650–700 nm) was added to the medium of the HuGE gastroids.

Image analysis

The damaged area was quantified from the timecourse of images as described previously (Aihara et al., 2014, 2013; Xue et al., 2010, 2011) using ImageJ and/or Metamorph software (ver. 6.3, Molecular Devices, Downington, PA). The damaged area was measured as the region with cellular loss of GFP fluorescence and/or NAD(P)H autofluorescence (*in vivo* animal model only). In each experiment, we determined the time point displaying maximal damage area and estimated rates of epithelial restitution starting from this time with a single exponential curve fit to the changing size of damaged area over time (Xue et al., 2010). Best fit values of the rate constant were used as estimates of the rate of restitution (units of min^{-1}). Additionally, movement of nuclei of the damaged cell was traced in the gastroid and plotted as the distance from the original position.

Actin dynamics were measured in the HuGE mouse. The GFP intensity was obtained from the leading edge adjacent to the damaged area in *in vivo* tissue, while it was measured in a more specific region, that is, lateral membrane or in the basal membrane adjacent to the damaged area in the *in vitro* gastroid. In control experiments, the GFP intensity was also measured in the cells located far away from the damage. The background-corrected GFP intensity was normalized to a value of 1 set for the averaged pre-damage baseline condition.

Intensity of Alexa Fluor 647-conjugated 10K-dextran or Lucifer Yellow was measured in the damaged area as well as in the medium. The background-corrected intensity in the damaged area was normalized to the background-corrected intensity in the medium.

Whole-mount staining

Gastroids with or without damage were fixed with 4% paraformaldehyde (PFA) for 30 min at room temperature. Gastroids were permeabilized with 1% Triton X-100 in PBS for 20 min, then blocked in 5% goat serum. Anti-ZO-1 antibody (1:100, Thermo Fisher Scientific, cat. #33-9100) were incubated overnight at 4°C. Then, gastroids were incubated with Alexa Fluor 647-conjugated goat anti-mouse IgG (1:200; Thermo Fisher Scientific, cat. #A21236) overnight at 4°C. Additionally, gastroids were incubated with Alexa Fluor 555–Phalloidin (1:40, Thermo Fisher Scientific, cat. #A34055) for 30 min, followed by nuclear stain (Hoechst 33342, 10 µg/ml, Thermo Fisher Scientific) for 20 min. Gastroids were imaged with Zeiss LSM710 confocal microscopy.

Model construction and simulation

The model components are summarized in the influence diagram presented in Fig. 2D. The influence diagram was converted into a system of ordinary differential equations. The first derivative of distance is the velocity, and the first derivatives of the velocity are the acceleration and de-acceleration. Given the unclear molecular nature of the assumed bi-stable switch, it is modelled with a generic formula as previously described (Mjolsness et al., 1991; Tyson and Novák, 2010; Zhang et al., 2013). The model parameters were estimated by comparing the temporal simulation of the models with the experimental data that is averaged from multiple observations. The temporal simulations and phase plots were carried out using XppAut (http://www.math.pitt.edu/~bard/xpp/xpp.html) and then plotted with MATLAB (https://mathworks.com/).

Statistical analysis

All values are reported from representative experiments as the mean±s.e.m. from multiple experiments. Statistical significance was determined using unpaired Student's *t*-test or one-way ANOVA with Dunnett's multiple comparison post-hoc test. A P value of <0.05 was considered significant.

Acknowledgements

We are grateful to Dr James E. Casanova (University of Virginia) for the gift of FAK inhibitors. We also gratefully acknowledge Dr Hans Clevers (Hubrecht Institute for Developmental Biology and Stem Cell Research, Netherlands) for the kind gift of Wnt secreting L-cells and noggin secreting cells. We also acknowledge Dr Jeffrey Whitsett for kindly donating the modified R-spondin secreting HEK-293T cells (Section of Neonatology, Perinatal and Pulmonary Biology, Cincinnati Children's Hospital Medical Center and The University of Cincinnati College of Medicine, Cincinnati, OH).

Competing interests

The authors declare no competing or financial interests.

Author contributions

Conceptualization: E.A., T.Z., M.H.M.; Methodology: E.A., T.Z.; Software: T.Z.; Validation: E.A., N.M.M.-C., H.H., A.L.M., K.A.E., T.Z.; Formal analysis: E.A., N.M.M.-C., H.H., A.L.M., K.A.E., T.Z.; Investigation: E.A., N.M.M.-C., H.H., A.L.M., K.A.E., T.Z.; Resources: C.B.G., W.W., J.T.; Writing - original draft: E.A., T.Z.; Writing - review & editing: E.A., T.Z., M.H.M.; Supervision: E.A., M.H.M.; Project administration: E.A., M.H.M.; Funding acquisition: E.A., W.W., M.H.M.

Funding

This work was supported by the National Institutes of Health (R01DK102551 to M.H.M., E.A.) and the Deutsche Forschungsgemeinschaft (DFG Priority Programme SPP1464 to W.W.). This project was also supported in part by the National Institutes of Health (P30 DK078392; Live Microscopy Core of the Digestive Disease Research Core Center in Cincinnati). Deposited in PMC for release after 12 months.

Supplementary information

Supplementary information available online at
http://jcs.biologists.org/lookup/doi/10.1242/jcs.216317.supplemental

References

Abreu-Blanco, M. T., Verboon, J. M. and Parkhurst, S. M. (2011). Cell wound repair in Drosophila occurs through three distinct phases of membrane and cytoskeletal remodeling. *J. Cell Biol.* **193**, 455-464.

Agle, K. A., Vongsa, R. A. and Dwinell, M. B. (2010). Calcium mobilization triggered by the chemokine CXCL12 regulates migration in wounded intestinal epithelial monolayers. *J. Biol. Chem.* **285**, 16066-16075.

Aihara, E. and Montrose, M. H. (2014). Importance of Ca(2+) in gastric epithelial restitution-new views revealed by real-time in vivo measurements. *Curr. Opin. Pharmacol.* **19**, 76-83.
Aihara, E., Hentz, C. L., Korman, A. M., Perry, N. P. J., Prasad, V., Shull, G. E. and Montrose, M. H. (2013). In vivo epithelial wound repair requires mobilization of endogenous intracellular and extracellular calcium. *J. Biol. Chem.* **288**, 33585-33597.
Aihara, E., Closson, C., Matthis, A. L., Schumacher, M. A., Engevik, A. C., Zavros, Y., Ottemann, K. M. and Montrose, M. H. (2014). Motility and chemotaxis mediate the preferential colonization of gastric injury sites by Helicobacter pylori. *PLoS Pathog.* **10**, e1004275.
Aihara, E., Engevik, K. A. and Montrose, M. H. (2017). Trefoil factor peptides and gastrointestinal function. *Annu. Rev. Physiol.* **79**, 357-380.
Antunes, M., Pereira, T., Cordeiro, J. V., Almeida, L. and Jacinto, A. (2013). Coordinated waves of actomyosin flow and apical cell constriction immediately after wounding. *J. Cell Biol.* **202**, 365-379.
Banan, A., Wang, J. Y., McCormack, S. A. and Johnson, L. R. (1996). Relationship between polyamines, actin distribution, and gastric healing in rats. *Am. J. Physiol.* **271**, G893-G903.
Bartfeld, S. and Clevers, H. (2017). Stem cell-derived organoids and their application for medical research and patient treatment. *J. Mol. Med.* **95**, 729-738.
Bement, W. M., Forscher, P. and Mooseker, M. S. (1993). A novel cytoskeletal structure involved in purse string wound closure and cell polarity maintenance. *J. Cell Biol.* **121**, 565-578.
Bieling, P., Li, T.-D., Weichsel, J., McGorty, R., Jreij, P., Huang, B., Fletcher, D. A. and Mullins, R. D. (2016). Force feedback controls motor activity and mechanical properties of self-assembling branched actin networks. *Cell* **164**, 115-127.
Byrne, K. M., Monsefi, N., Dawson, J. C., Degasperi, A., Bukowski-Wills, J.-C., Volinsky, N., Dobrzyński, M., Birtwistle, M. R., Tsyganov, M. A., Kiyatkin, A. et al. (2016). Bistability in the Rac1, PAK, and RhoA signaling network drives actin cytoskeleton dynamics and cell motility switches. *Cell Syst.* **2**, 38-48.
Cooper, J. A. (1987). Effects of cytochalasin and phalloidin on actin. *J. Cell Biol.* **105**, 1473-1478.
Critchlow, J., Magee, D., Ito, S., Takeuchi, K. and Silen, W. (1985). Requirements for restitution of the surface epithelium of frog stomach after mucosal injury. *Gastroenterology* **88**, 237-249.
Demitrack, E. S., Soleimani, M. and Montrose, M. H. (2010). Damage to the gastric epithelium activates cellular bicarbonate secretion via SLC26A9 Cl(−)/HCO(3)(−). *Am. J. Physiol. Gastrointest. Liver Physiol.* **299**, G255-G264.
Gagliardi, P. A., Somale, D., Puliafito, A., Chiaverina, G., di Blasio, L., Oneto, M., Bianchini, P., Bussolino, F. and Primo, L. (2018). MRCKalpha is activated by caspase cleavage to assemble an apical actin ring for epithelial cell extrusion. *J. Cell Biol.* **217**, 231-249.
Gonzalez-Mariscal, L., Contreras, R. G., Bolivar, J. J., Ponce, A., Chavez De Ramirez, B. and Cereijido, M. (1990). Role of calcium in tight junction formation between epithelial cells. *Am. J. Physiol.* **259**, C978-C986.
Goode, B. L. and Eck, M. J. (2007). Mechanism and function of formins in the control of actin assembly. *Annu. Rev. Biochem.* **76**, 593-627.
Gurniak, C. B. and Witke, W. (2007). HuGE, a novel GFP-actin-expressing mouse line for studying cytoskeletal dynamics. *Eur. J. Cell Biol.* **86**, 3-12.
Hall, A. (1998). Rho GTPases and the actin cytoskeleton. *Science* **279**, 509-514.
Hunter, M. V., Lee, D. M., Harris, T. J. C. and Fernandez-Gonzalez, R. (2015). Polarized E-cadherin endocytosis directs actomyosin remodeling during embryonic wound repair. *J. Cell Biol.* **210**, 801-816.
Kueh, H. Y., Charras, G. T., Mitchison, T. J. and Brieher, W. M. (2008). Actin disassembly by cofilin, coronin, and Aip1 occurs in bursts and is inhibited by barbed-end cappers. *J. Cell Biol.* **182**, 341-353.
Kuipers, D., Mehonic, A., Kajita, M., Peter, L., Fujita, Y., Duke, T., Charras, G. and Gale, J. E. (2014). Epithelial repair is a two-stage process driven first by dying cells and then by their neighbours. *J. Cell Sci.* **127**, 1229-1241.
Lecuit, T. and Yap, A. S. (2015). E-cadherin junctions as active mechanical integrators in tissue dynamics. *Nat. Cell Biol.* **17**, 533-539.
Levayer, R. and Lecuit, T. (2012). Biomechanical regulation of contractility: spatial control and dynamics. *Trends Cell Biol.* **22**, 61-81.
Lomakin, A. J., Lee, K.-C., Han, S. J., Bui, D. A., Davidson, M., Mogilner, A. and Danuser, G. (2015). Competition for actin between two distinct F-actin networks defines a bistable switch for cell polarization. *Nat. Cell Biol.* **17**, 1435-1445.
Lubkov, V. and Bar-Sagi, D. (2014). E-cadherin-mediated cell coupling is required for apoptotic cell extrusion. *Curr. Biol.* **24**, 868-874.
Machacek, M., Hodgson, L., Welch, C., Elliott, H., Pertz, O., Nalbant, P., Abell, A., Johnson, G. L., Hahn, K. M. and Danuser, G. (2009). Coordination of Rho GTPase activities during cell protrusion. *Nature* **461**, 99-103.
Mahe, M. M., Aihara, E., Schumacher, M. A., Zavros, Y., Montrose, M. H., Helmrath, M. A., Sato, T. and Shroyer, N. F. (2013). Establishment of gastrointestinal epithelial organoids. *Curr. Protoc. Mouse Biol.* **3**, 217-240.
Marchiando, A. M., Shen, L., Graham, W. V., Edelblum, K. L., Duckworth, C. A., Guan, Y., Montrose, M. H., Turner, J. R. and Watson, A. J. (2011). The epithelial barrier is maintained by in vivo tight junction expansion during pathologic intestinal epithelial shedding. *Gastroenterology* **140**, 1208-1218.e1-2.
Matsuoka, T. and Yashiro, M. (2014). Rho/ROCK signaling in motility and metastasis of gastric cancer. *World J. Gastroenterol.* **20**, 13756-13766.
Michael, M., Meiring, J. C. M., Acharya, B. R., Matthews, D. R., Verma, S., Han, S. P., Hill, M. M., Parton, R. G., Gomez, G. A. and Yap, A. S. (2016). Coronin 1B reorganizes the architecture of F-actin networks for contractility at steady-state and apoptotic Adherens junctions. *Dev. Cell* **37**, 58-71.
Mitra, S. K., Hanson, D. A. and Schlaepfer, D. D. (2005). Focal adhesion kinase: in command and control of cell motility. *Nat. Rev. Mol. Cell Biol.* **6**, 56-68.
Mjolsness, E., Sharp, D. H. and Reinitz, J. (1991). A connectionist model of development. *J. Theor. Biol.* **152**, 429-453.
Monier, B., Gettings, M., Gay, G., Mangeat, T., Schott, S., Guarner, A. and Suzanne, M. (2015). Apico-basal forces exerted by apoptotic cells drive epithelium folding. *Nature* **518**, 245-248.
Mueller, J., Szep, G., Nemethova, M., de Vries, I., Lieber, A. D., Winkler, C., Kruse, K., Small, J. V., Schmeiser, C., Keren, K. et al. (2017). Load adaptation of Lamellipodial actin networks. *Cell* **171**, 188-200.e16.
Munjal, A., Philippe, J.-M., Munro, E. and Lecuit, T. (2015). A self-organized biomechanical network drives shape changes during tissue morphogenesis. *Nature* **524**, 351-355.
Nguyen, T., Chai, J., Li, A., Akahoshi, T., Tanigawa, T. and Tarnawski, A. S. (2007). Novel roles of local insulin-like growth factor-1 activation in gastric ulcer healing: promotes actin polymerization, cell proliferation, re-epithelialization, and induces cyclooxygenase-2 in a phosphatidylinositol 3-kinase-dependent manner. *Am. J. Pathol.* **170**, 1219-1228.
Osada, T., Watanabe, S., Tanaka, H., Hirose, M., Miyazaki, A. and Sato, N. (1999). Effect of mechanical strain on gastric cellular migration and proliferation during mucosal healing: role of Rho dependent and Rac dependent cytoskeletal reorganisation. *Gut* **45**, 508-515.
Paehler Vor der Nolte, A., Chodisetti, G., Yuan, Z., Busch, F., Riederer, B., Luo, M., Yu, Y., Menon, M. B., Schneider, A., Stripecke, R. et al. (2017). Na+ /H+ exchanger NHE1 and NHE2 have opposite effects on migration velocity in rat gastric surface cells. *J. Cell. Physiol.* **232**, 1669-1680.
Pai, R., Szabo, I. L., Giap, A. Q., Kawanaka, H. and Tarnawski, A. S. (2001). Nonsteroidal anti-inflammatory drugs inhibit re-epithelialization of wounded gastric monolayers by interfering with actin, Src, FAK, and tensin signaling. *Life Sci.* **69**, 3055-3071.
Pellegrin, S. and Mellor, H. (2007). Actin stress fibres. *J. Cell Sci.* **120**, 3491-3499.
Peng, G. E., Wilson, S. R. and Weiner, O. D. (2011). A pharmacological cocktail for arresting actin dynamics in living cells. *Mol. Biol. Cell* **22**, 3986-3994.
Pollard, T. D. (2007). Regulation of actin filament assembly by Arp2/3 complex and formins. *Annu. Rev. Biophys. Biomol. Struct.* **36**, 451-477.
Priya, R., Gomez, G. A., Budnar, S., Verma, S., Cox, H. L., Hamilton, N. A. and Yap, A. S. (2015). Feedback regulation through myosin II confers robustness on RhoA signalling at E-cadherin junctions. *Nat. Cell Biol.* **17**, 1282-1293.
Ranta-Knuuttila, T., Kiviluoto, T., Mustonen, H., Puolakkainen, P., Watanabe, S., Sato, N. and Kivilaakso, E. (2002). Migration of primary cultured rabbit gastric epithelial cells requires intact protein kinase C and Ca2+/calmodulin activity. *Dig. Dis. Sci.* **47**, 1008-1014.
Rao, J. N., Liu, S. V., Zou, T., Liu, L., Xiao, L., Zhang, X., Bellavance, E., Yuan, J. X.-J. and Wang, J.-Y. (2008). Rac1 promotes intestinal epithelial restitution by increasing Ca2+ influx through interaction with phospholipase C-(gamma)1 after wounding. *Am. J. Physiol. Cell Physiol.* **295**, C1499-C1509.
Russo, J. M., Florian, P., Shen, L., Graham, W. V., Tretiakova, M. S., Gitter, A. H., Mrsny, R. J. and Turner, J. R. (2005). Distinct temporal-spatial roles for rho kinase and myosin light chain kinase in epithelial purse-string wound closure. *Gastroenterology* **128**, 987-1001.
Sato, T., Vries, R. G., Snippert, H. J., van de Wetering, M., Barker, N., Stange, D. E., van Es, J. H., Abo, A., Kujala, P., Peters, P. J. et al. (2009). Single Lgr5 stem cells build crypt-villus structures in vitro without a mesenchymal niche. *Nature* **459**, 262-265.
Schumacher, M. A., Aihara, E., Feng, R., Engevik, A., Shroyer, N. F., Ottemann, K. M., Worrell, R. T., Montrose, M. H., Shivdasani, R. A. and Zavros, Y. (2015a). The use of murine-derived fundic organoids in studies of gastric physiology. *J. Physiol.* **593**, 1809-1827.
Schumacher, M. A., Feng, R., Aihara, E., Engevik, A. C., Montrose, M. H., Ottemann, K. M. and Zavros, Y. (2015b). Helicobacter pylori-induced Sonic Hedgehog expression is regulated by NFkappaB pathway activation: the use of a novel in vitro model to study epithelial response to infection. *Helicobacter* **20**, 19-28.
Spector, I., Shochet, N. R., Kashman, Y. and Groweiss, A. (1983). Latrunculins: novel marine toxins that disrupt microfilament organization in cultured cells. *Science* **219**, 493-495.
Stange, D. E., Koo, B.-K., Huch, M., Sibbel, G., Basak, O., Lyubimova, A., Kujala, P., Bartfeld, S., Koster, J., Geahlen, J. H. et al. (2013). Differentiated Troy+ chief cells act as reserve stem cells to generate all lineages of the stomach epithelium. *Cell* **155**, 357-368.
Starodub, O. T., Demitrack, E. S., Baumgartner, H. K. and Montrose, M. H. (2008). Disruption of the Cox-1 gene slows repair of microscopic lesions in the mouse gastric epithelium. *Am. J. Physiol. Cell Physiol.* **294**, C223-C232.

Stricker, J., Falzone, T. and Gardel, M. L. (2010). Mechanics of the F-actin cytoskeleton. *J. Biomech.* **43**, 9-14.

Szabó, I. L., Pai, R., Jones, M. K., Ehring, G. R., Kawanaka, H. and Tarnawski, A. S. (2002). Indomethacin delays gastric restitution: association with the inhibition of focal adhesion kinase and tensin phosphorylation and reduced actin stress fibers. *Exp. Biol. Med.* **227**, 412-424.

Tamada, M., Perez, T. D., Nelson, W. J. and Sheetz, M. P. (2007). Two distinct modes of myosin assembly and dynamics during epithelial wound closure. *J. Cell Biol.* **176**, 27-33.

Tyson, J. J. and Novák, B. (2010). Functional motifs in biochemical reaction networks. *Annu. Rev. Phys. Chem.* **61**, 219-240.

Watanabe, S., Hirose, M., Yasuda, T., Miyazaki, A. and Sato, N. (1994a). Role of actin and calmodulin in migration and proliferation of rabbit gastric mucosal cells in culture. *J. Gastroenterol. Hepatol.* **9**, 325-333.

Watanabe, S., Wang, X. E., Hirose, M. and Sato, N. (1994b). Effect of myosin light chain kinase inhibitor wortmannin on the wound repair of cultured gastric mucosal cells. *Biochem. Biophys. Res. Commun.* **199**, 799-806.

Xu, L.-F., Xu, C., Mao, Z.-Q., Teng, X., Ma, L. and Sun, M. (2011). Disruption of the F-actin cytoskeleton and monolayer barrier integrity induced by PAF and the protective effect of ITF on intestinal epithelium. *Arch. Pharm. Res.* **34**, 245-251.

Xue, L., Aihara, E., Podolsky, D. K., Wang, T. C. and Montrose, M. H. (2010). In vivo action of trefoil factor 2 (TFF2) to speed gastric repair is independent of cyclooxygenase. *Gut* **59**, 1184-1191.

Xue, L., Aihara, E., Wang, T. C. and Montrose, M. H. (2011). Trefoil factor 2 requires Na/H exchanger 2 activity to enhance mouse gastric epithelial repair. *J. Biol. Chem.* **286**, 38375-38382.

Yanaka, A., Suzuki, H., Shibahara, T., Matsui, H., Nakahara, A. and Tanaka, N. (2002). EGF promotes gastric mucosal restitution by activating Na(+)/H(+) exchange of epithelial cells. *Am. J. Physiol. Gastrointest. Liver Physiol.* **282**, G866-G876.

Zhang, T., Oliveira, R. A., Schmierer, B. and Novák, B. (2013). Dynamical scenarios for chromosome bi-orientation. *Biophys. J.* **104**, 2595-2606.

Zhao, X. and Guan, J.-L. (2011). Focal adhesion kinase and its signaling pathways in cell migration and angiogenesis. *Adv. Drug Delivery. Rev.* **63**, 610-615.

Zuo, Y., Shields, S.-K. and Chakraborty, C. (2006). Enhanced intrinsic migration of aggressive breast cancer cells by inhibition of Rac1 GTPase. *Biochem. Biophys. Res. Commun.* **351**, 361-367.